ADVANCED ENERGY MATERIALS
www.advenergymat.de

Tailoring Microenvironments and In Situ Transformations of Cu Catalysts for Selective and Stable Electrosynthesis of Multicarbon Products

*Pan Ding, Julius Kühne, Saswati Santra, Richard Zell, Philipp Zellner, Tim Rieth, Jianyong Gao, Jianian Chen, Guanda Zhou, Johannes Dittloff, Knut Müller-Caspary, and Ian D. Sharp**

Electrochemical CO_2 reduction is of tremendous interest for storing chemical energy from renewable sources while reducing CO_2 emissions. While copper is one of the most effective catalysts, it suffers from low selectivity and limited long-term durability. Here, these limitations are overcome by engineering Nafion coatings on CuO nanoparticle-based catalysts supported on glassy carbon. By tuning the Nafion thickness and internal structure, it is shown that both the selectivity to multicarbon (C_{2+}) products and long-term stability can be dramatically enhanced. Optimized catalyst layers reach Faradaic efficiencies for C_{2+} products of 86% during long-term testing for 200 h, with no evidence for performance degradation. Indeed, the C_{2+} Faradaic efficiency increases during testing, which is attributed to favorable in situ electrochemical fragmentation of catalytic nanoparticles. Finally, the optimized Nafion/Cu catalytic coatings are utilized to create scalable membrane electrode assemblies for CO_2 electrolysis, yielding significantly enhanced C_2H_4 selectivity (≈58%) and activity at technologically-relevant currents of 1–2 A. These results highlight the potential for creating multi-functional Nafion coatings on CO_2 reduction catalysts to favorably tune the reaction environment, while also promoting in situ transformations to active and selective nanoscale structures and morphologies, not just on model surfaces but also in state-of-the-art gas diffusion electrodes.

1. Introduction

Electrochemical CO_2 reduction (CO_2R) to value-added feedstock chemicals using electricity from renewable energy is of considerable interest in the current transition to a carbon-neutral society.[1] A number of metal-based electrocatalysts have been developed to catalyze CO_2 reduction reactions (CO_2RR) in aqueous solutions. Among them, copper (Cu)-based materials have received the most attention due to their unique ability to produce a range of multicarbon (C_{2+}) products, including ethylene (C_2H_4), ethanol (C_2H_5OH), acetate (CH_3COO^-), and n-propanol (C_3H_7OH).[2] Despite intensive efforts to optimize Cu-catalyzed CO_2RR over the past decades, the low selectivity toward desired value-added chemicals and their poor long-term durability remain critical challenges.[3,4] Overcoming these challenges is particularly difficult due to the complex reaction network associated with CO_2 electrolysis, in which subtle modifications of the catalytic system during continuous operation can lead to substantial changes in the product distribution, often resulting in increasing production of hydrogen at the cost of valuable C_{2+} products. Indeed, both the structure of Cu-based catalysts and the local reaction environment near the catalyst surface have significant impacts on selective electrosynthesis of C_{2+} products in CO_2RR.[2] Flat Cu foils tend to favor generation of single carbon products, especially

P. Ding, J. Kühne, S. Santra, P. Zellner, T. Rieth, J. Gao, J. Chen, G. Zhou, J. Dittloff, I. D. Sharp
Walter Schottky Institute
Technical University of Munich
Am Coulombwall 4, 85748 Garching, Germany
E-mail: sharp@wsi.tum.de

The ORCID identification number(s) for the author(s) of this article can be found under https://doi.org/10.1002/aenm.202303936

DOI: 10.1002/aenm.202303936

P. Ding, J. Kühne, S. Santra, P. Zellner, T. Rieth, J. Gao, J. Chen, G. Zhou, J. Dittloff, I. D. Sharp
Physics Department
TUM School of Natural Sciences
Technical University of Munich
Am Coulombwall 4, 85748 Garching, Germany

R. Zell, K. Müller-Caspary
Department of Chemistry and Center for NanoScience
Ludwig-Maximilians-Universität München
Butenandtstr. 11, 81377 Munich, Germany

methane (CH_4), rather than multicarbon products.[5] In contrast, rough Cu structures, often formed via the reduction of copper oxides or the electrochemical reconstruction of initially smooth surfaces, display particularly high selectivities toward C_{2+} products. Such surfaces are characterized by an abundance of undercoordinated sites that can strongly bind important intermediates, such as *CO, thereby enhancing C-C coupling.[6,7] Moreover, the C_{2+} selectivity can be tuned by varying the size and shape/facet of Cu nanostructures. For example, a high Faradaic efficiency (FE) of 41% for C_2H_4 has been demonstrated on Cu nanocubes with an optimal size of 44 nm.[8]

In addition to the engineering of catalyst structures and morphologies, C_{2+} selectivity can be further enhanced by modifying the reaction microenvironment, including the electrolyte cation, pH, and molar ratio of CO_2/H_2O in the vicinity of the Cu surface. For example, compared to larger hydrated cations of Li^+, Na^+, and K^+, smaller hydrated ions of Cs^+ and Rb^+ induce a larger surface charge density and stronger interfacial electric field, which enhances adsorption of CO_2 and C_{2+} intermediates, thereby facilitating C_{2+} production.[9] Furthermore, recent studies have shown that adjusting the local pH and CO_2/H_2O availability by tailoring organic coatings (binders or ion conductive polymers, ionomers) on Cu also influences the activity and selectivity of CO_2RR. In particular, increasing the hydrophobicity of organic binder coatings can enhance the local OH^- concentration and CO_2/H_2O concentration ratio, which contributes to improved selectivity.[10–12] In another example, a double layer of both anion- and cation-conducting ionomers was introduced on the Cu surface to regulate the water concentration and to increase local pH by trapping hydroxide ions (OH^-), which resulted in significant suppression of the hydrogen evolution reaction (HER) and a record high 90% Faradaic efficiency of C_{2+} products.[13]

Alongside product selectivity, the poor long-term durability of Cu-based catalysts introduces another significant barrier to sustainable generation of C_{2+} products from CO_2R. Indeed, bare Cu-based catalysts have been shown to be unstable when subjected to continuous CO_2 electrolysis. Severe structural and morphological changes of catalyst layers, including their delamination from substrates, the agglomeration of catalyst particles, and facet reconstruction, lead to degradation of catalytic performance.[14] Therefore, it is of crucial importance to develop strategies to improve the durability of Cu-based catalysts for selective synthesis of C_{2+} products.

Although various inorganic or organic coatings have been explored to enhance both the C_{2+} product selectivity and stability of Cu-based catalysts,[11,15] understanding the impact of the most widely used binder–Nafion–is only now emerging.[12,16–23] Recently, we reported that the activity, selectivity, and stability of CO_2R can be drastically impacted by engineering the internal structure and properties of Nafion ionomer coatings on oxide-derived Cu catalysts supported on carbon paper.[24] Importantly, thin layers of Nafion can beneficially stabilize the catalyst and create favorable microenvironments for CO_2R, but can also lead to the blocking of active sites or introduce undesired mass transport limitations. In that previous study, we found that increasing the solvent dielectric constant by increasing the water content leads to thinner Nafion coatings with improved network connectivity, which results in an increased molar ratio $[CO_2]/[H_2O]$ and, thus, increased CO_2 availability and suppressed HER.[24] In addition, the reduced water content within the Nafion films may have a significant impact on the local pH, yielding more alkaline microenvironments that promote C-C coupling. While that study provided important insights into the function of Nafion binders for CO_2R and demonstrated a generalizable approach to optimizing different reaction outcomes via modification of catalyst ink formulations, the complex microporous structure of the carbon paper support may have contributed to a broadened distribution of reaction microenvironments near its surface and deeper within its pores, which could limit the Faradaic efficiency to selected high value products. Therefore, in the present work, we first apply the Nafion/solvent engineering strategy to well-defined and planar glassy carbon substrates in H-type cells, showing that the resulting Nafion/CuO nanoparticle coatings yield significantly enhanced C_{2+} product selectivity with exceptional long-term stability during sustained durability testing. In addition, we show that the optimized Nafion/Cu catalytic coatings can be translated to scalable gas-fed membrane electrode assemblies (MEAs) featuring enhanced production of C_{2+} products under industry-relevant operating conditions. For the H-cell configuration, optimized catalyst layers on glassy carbon are shown to yield stable and highly selective electrosynthesis of C_{2+} products, with maximum C_2H_4 FE of 65% and total C_{2+} FEs of 86% during long-term CO_2 electrolysis for at least 200 h. Remarkably, the selectivity of C_{2+} products is found to increase during the 200 h performance test, which is attributed to in situ electrochemical fragmentation of catalyst particles and the favorable reaction microenvironment provided by Nafion coatings prepared from inks containing optimal Nafion contents and solvent compositions. This behavior stands in contrast to most previous reports of Cu-based CO_2R catalysts, in which long-term operation frequently leads to increased hydrogen evolution at the cost of reduced CO_2RR selectivity. Importantly, integration of these Nafion/Cu nanoparticle coatings into scalable gas-fed MEAs via spray coating of the optimized catalyst inks also results in highly selective and active production of C_{2+} products, with the C_2H_4 FE and partial current density peaking at 58% and 136 mA cm^{-2}, respectively. Together, these results reveal the importance of engineering multi-functional Nafion coatings that not only provide favorable microenvironments and stabilize electrochemically active interfaces against degradation, but also promote in situ transformations to desirable nanoscale structures and morphologies, thereby enabling highly selective and stable CO_2R in H-cell and integrated gas diffusion electrode (GDE) configurations alike.

2. Results and Discussion

2.1. Effect of Catalyst Ink Composition on CO_2 Electrolysis

As a starting point for understanding and controlling the activity of Cu-based catalysts, we first compare their morphologies and CO_2 electrolysis characteristics in the presence and absence of Nafion ionomer. Using commercial CuO nanoparticles (NPs) as the model pre-catalyst, we utilized various ink compositions containing four different Nafion weight ratios (0, 0.005, 0.05, and 0.5 wt%) and two water volume fractions (0 and 50 vol%, with isopropanol as balance of solvent). Following preparation of the inks, working electrodes were fabricated by drop casting catalyst layers on glassy carbon substrates with a constant mass loading

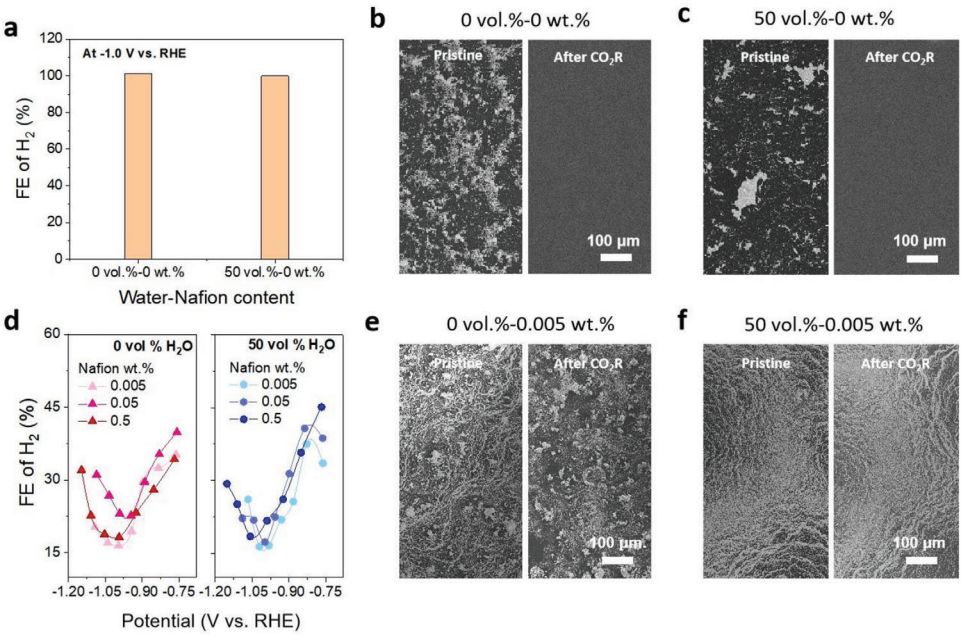

Figure 1. Electrochemical and structural characterization of electrodes prepared from inks with different Nafion/solvent compositions. a–c) The average Faradaic efficiencies (FEs) of H_2 during 1 h chronoamperometric CO_2 electrolysis at -1.0 V vs. RHE on electrodes produced in the absence of Nafion, with ink compositions of 0 vol% H_2O-0 wt% Nafion and 50 vol% H_2O-0 wt% Nafion (a) and corresponding SEM images of the electrodes before and after CO_2 electrolysis (b, c). d–f) The potential-dependent H_2 FEs during chronoamperometric CO_2 electrolysis on electrodes produced from inks possessing two H_2O volume fractions (0 and 50 vol%) and three Nafion weight fractions (0.005, 0.05, and 0.5 wt%) of Nafion (d), along with the corresponding SEM images of electrodes obtained before and after CO_2 electrolysis (e,f).

of 0.255 mg cm^{-2}. Throughout this work, the prepared Nafion coatings and catalyst layers are denoted by their volumetric water content in solvent-Nafion weight ratio in the form of, for example, 50 vol%-0.5 wt%.

X-ray diffraction (XRD) data and scanning electron microscopy (SEM) images demonstrate that the pre-catalytic nanoparticles comprise pure monoclinic phase CuO and have an average size of ≈50 nm, respectively (Figures S1 and S2, Supporting Information). In the absence of Nafion, large aggregates of CuO NPs and extended regions of bare glassy carbon are observed, regardless of the water content in the solvent. In contrast, addition of Nafion into the catalyst inks leads to significantly suppressed particle aggregation and more uniform CuO NP coatings (Figure S2, Supporting Information). Notably, the homogeneity of the catalyst layers increases with increasing Nafion content in the ink, yielding the smoothest and most uniform films for those prepared with 0.5 wt% Nafion. This result is consistent with our prior findings, indicating the importance of Nafion in the catalyst ink for producing stable dispersions and suppressing NP agglomeration upon catalyst layer formation.[24] In addition, magnified SEM images for a fixed Nafion content of 0.25 wt% indicate the presence of thicker Nafion coatings around CuO NPs with decreasing water content in the solvent (Figure S3, Supporting Information). Complementary measurements of the double layer capacitances of these electrodes reveal a reduction of the electrochemically active surface area (ECSA) with decreasing water content (Figure S4, Supporting Information), suggesting the blocking of catalyst surfaces as the Nafion thickness increases. These observations are consistent with the known dependence of the internal Nafion structure on solvent polarity. In particular, the increasing solvent dielectric constant with increasing water fraction promotes strong interactions between the hydrophobic perfluorocarbon backbones of Nafion, resulting in thinner films possessing improved inner network connectivity.[14,18] In this regard, the presence of Nafion in the solvent ink is necessary to suppress CuO NP agglomeration and obtain uniform catalyst layers, whereas increasing water content in the solvent is beneficial for maintaining thin Nafion coatings with internal structures that permit facile mass transport without blocking surface active sites.

We next examine the CO_2R activities and selectivities of working electrodes prepared from catalyst inks with different solvent and Nafion contents in CO_2-saturated 0.1 M $KHCO_3$ aqueous solutions using an H-type cell. Gaseous products were analyzed by online gas chromatography during 1 h of chronoamperometric testing at each fixed potential. Remarkably, electrodes prepared with Nafion-free inks exhibited negligible activity for CO_2R, with H_2 being the only major product detected. As shown in **Figure 1a**, the measured average FEs of H_2 were ≈100% for both Nafion-free electrodes, regardless of solvent composition, as measured at -1.0 V vs. the reversible hydrogen electrode (V_{RHE}). To understand this surprising behavior, we performed post-mortem SEM imaging, which revealed the complete absence of catalyst layers on the glassy carbon surfaces after sustained operation (Figure 1b,c). Thus, we conclude that poor adhesion of Nafion-free Cu NP films results in exfoliation of catalyst layers from substrates and, consequently, complete loss of CO_2R activity.

In sharp contrast, electrodes prepared with Nafion-containing formulations exhibited much lower FEs (i.e., <45%) for H_2 production across a wide potential range, suggesting the possibility

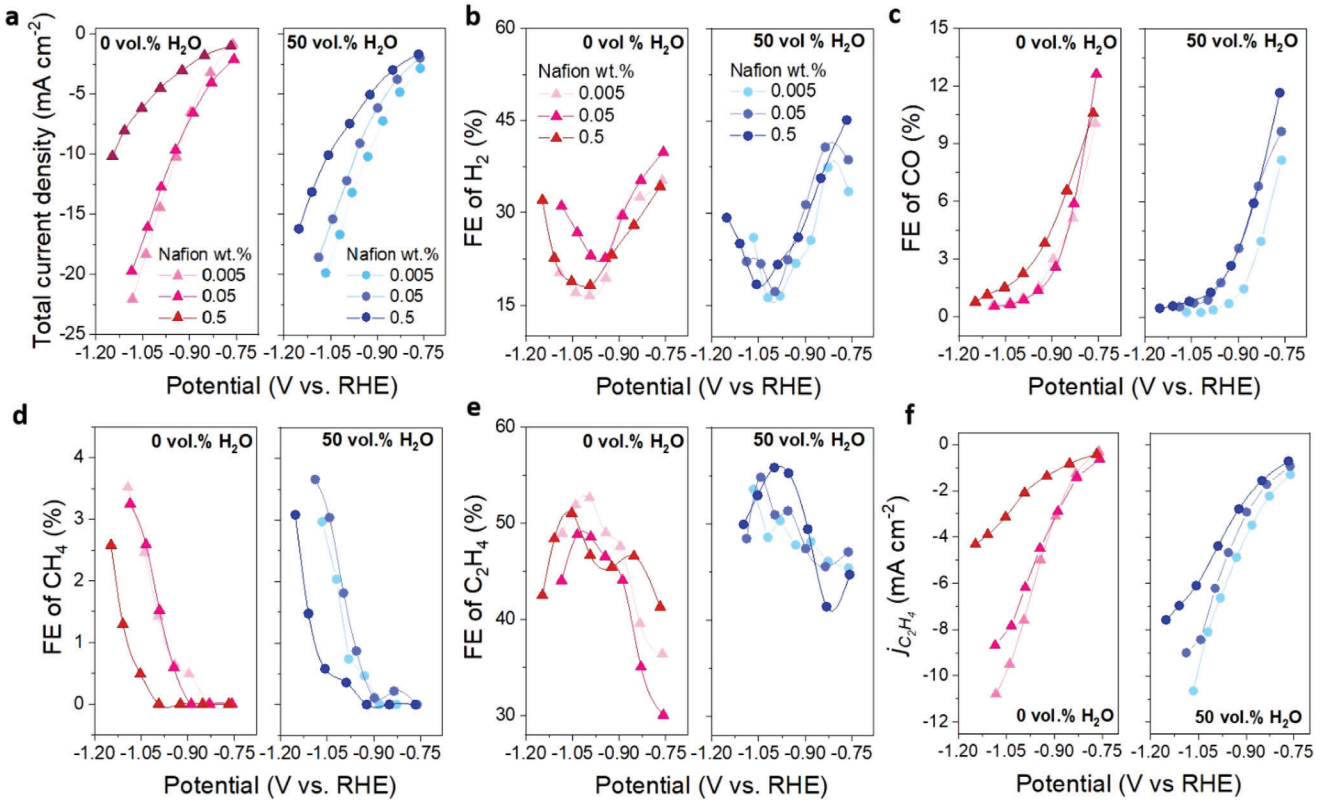

Figure 2. Effect of the composition of Nafion/solvent inks on potential-dependent CO_2 electrolysis. The catalytic performance of electrodes prepared from inks containing different Nafion (0.005, 0.05, and 0.5 wt%) and H_2O/isopropanol (0 and 50 vol% H_2O) contents, evaluated in terms of total current density a), as well as Faradaic efficiencies for H_2 b), CO c), CH_4 d), and C_2H_4 e), as well as the partial current density of C_2H_4 f).

for appreciable generation of CO_2R products (Figure 1d). Indeed, the minimum H_2 FE of <20% near -1.0 V_{RHE} indicates significant suppression of HER upon addition of Nafion. Consistent with this observation, post-mortem analysis reveals that catalyst layers were preserved with no significant exposure of the underlying glassy carbon substrates after the complete set of chronoamperometric tests on all Nafion-containing electrodes (Figure 1e,f; Figure S5, Supporting Information). Such considerable stability variations between Nafion-free and Nafion-containing electrodes underscore the necessity of incorporating Nafion in catalyst inks to ensure robust electrodes with strong interaction between catalyst layers and substrates. Furthermore, we note that this behavior differs from previous experiments with Nafion-free CuO NPs on porous carbon paper substrates,[24] where significant catalyst restructuring was observed but catalytic CO_2R activity was retained even in the absence of Nafion. This difference indicates the challenge of stabilizing catalytic NPs on planar surfaces, as well as the ability of porous supports to inhibit catalyst detachment due to physical confinement. Thus, we conclude that Nafion plays an especially important role in ensuring the durability of catalyst layers on planar supports, such as the glassy carbon substrates used here.

To quantify the dependence of CO_2R performance on the catalyst ink composition, potential-dependent total current densities (TCDs), FEs, and the partial current density for individual products were analyzed during chronoamperometric testing of 5 h, as shown in **Figures** 2 and S6 (Supporting Information). Overall, the TCDs increased with decreasing Nafion content in the catalyst ink (Figure 2a). The maximum TCDs of ≈-20 mA cm^{-2} near -1.05 V_{RHE} were achieved at the lowest Nafion content of 0.005 wt%, regardless of water content in solvent. However, for the highest Nafion content of 0.5 wt%, the electrode prepared with 50 vol% water exhibited significantly larger TCDs across the entire potential range than the analogous one prepared without water. We ascribe this enhanced TCD at higher water content to the larger electrochemically active surface areas of catalyst layers produced from high water content inks, as previously reported and discussed above.[24]

The potential-dependent FEs of gaseous products from the set of cathodes prepared from different solvent ink compositions are plotted in Figure 2b–e and Figure S6 (Supporting Information). For all electrodes, C_2H_4 and H_2 were detected as two major products. While HER was significantly suppressed near -1.0 V_{RHE}, reaching a minimum H_2 FE of ≈16% for most electrodes, a high C_2H_4 FE was observed near this working potential. In general, higher C_2H_4 FEs and larger partial current densities of C_2H_4 were observed on electrodes prepared from high water content solvents relative to those prepared with water-free formulations. Indeed, a maximum C_2H_4 FE of ≈60% at -1.05 V_{RHE} was observed from the electrode prepared from the 50 vol% H_2O-0.5 wt% Nafion catalyst ink. However, this beneficial improvement of selectivity appears to come at the cost of reduced activity, with the partial current densities of C_2H_4 decreasing with increasing Nafion content (Figure 2f). Nevertheless, the magnitude of

the activity loss is reduced with increasing water content, thus motivating further exploration of higher-water-content formulations to improve the activity of producing C_2H_4 or other C_{2+} products, as described in the next section below.

Alongside C_2H_4 and H_2, CO and CH_4 were also detected as minor products, with increasing Nafion content leading to somewhat increasing CO FEs and decreasing CH_4 FEs across the investigated potential range (Figure 2c,d). In particular, at -1.05 V_{RHE}, where the C_2H_4 FE was maximized, the CO FEs were less than 1% on all electrodes, while CH_4 FEs were <1% on electrodes prepared from inks with the highest Nafion content (0.5 wt%). We note that the CH_4 FE has been reported to be an indicator for local pH in CO_2 electrolysis, as the production of one CH_4 molecule from CO_2 requires the consumption of 8 protons.[25] The extremely low CH_4 FE measured on electrodes prepared with the highest Nafion content implies that thicker Nafion coatings result in higher local pH, thus suppressing HER and promoting the selectivity of C_{2+} products.[13,25,26] In addition, the overall increase of C_2H_4 FE for films prepared with 50 vol% water compared to those prepared without water is consistent with the higher inner network connectivity afforded by the higher dielectric constant of the solvent, which has been shown to enhance the local CO_2/H_2O concentration and pH to favor C-C coupling reactions.

Overall, the catalyst ink composition-dependent CO_2R performance characteristics on the glassy carbon substrate are consistent with prior findings regarding the role of Nafion structure and thickness on the local reaction environment.[24] However, important differences between CO_2R on planar glassy carbon supports compared to previously reported findings on carbon paper supports are apparent.[24] In particular, use of glassy carbon leads to significantly greater suppression of H_2 and single carbon (C_1) product generation, along with a pronounced enhancement of C_{2+} products, particularly C_2H_4. While this could indicate that the planar system provides more homogeneous reaction microenvironments that promote higher C_{2+} selectivity, these results motivate a broader exploration of the substrate-specific trends of CO_2R performance on catalyst ink composition, with the aim of identifying optimal formulations to achieve necessary combinations of selectivity and stability, as described below.

2.2. Optimized Nafion/Solvent Compositions for Enhanced Generation of C_{2+} Products

As a next step, we systematically assessed the effect of catalyst ink composition on the selectivity of CO_2R during longer CO_2 electrolysis experiments, with the aim of identifying the conditions needed to maximize selective generation of C_{2+} products. For this purpose, a series of catalyst inks containing six Nafion weight fractions (0.005, 0.025, 0.05, 0.125, 0.25, and 0.5 wt%) and four solvent compositions (0, 25, 50, and 75 vol% H_2O, with isopropanol as the balance) were employed to produce working electrodes. All electrodes were subjected to 5 h chronopotentiometry tests at a constant current density of -12.8 mA cm^{-2} and both gas and liquid products, including H_2, CO, CH_4, C_2H_4, formate, ethanol, acetate, and n-propanol, were quantified. The current density was fixed at -12.8 mA cm^{-2}, which corresponds to an operating condition that yields lowest HER activity and highest FEs for C_2H_4 for the majority of electrodes described above (Figure 2). The resulting product distribution obtained from each of the 24 independent electrodes is shown in Figure S7 (Supporting Information). For all cases, the three major products were ethylene, ethanol, and hydrogen, with FEs that varied as a function of catalyst ink composition. All other analyzed compounds (CO, CH_4, formate, acetate, n-propanol) represented minor contributions (<10%) to the overall product distribution. The total FE for all products was ≈100% in all cases, indicating the lack of significant quantities of undetected products or corrosion currents.

To further analyze the influence of catalyst ink composition on the selectivity of each product, the average FEs were individually compared in heatmaps (**Figure 3a–c**; Figure S8, Supporting Information). For most catalyst ink compositions, the H_2 FE was maintained at a low level of ≈25%. However, for the case of high Nafion contents of 0.25 and 0.5 wt%, HER was highly dependent on water content. For example, vigorous HER with a H_2 FE of ≈40% was measured for the 0 vol%-0.5 wt% sample, but was significantly reduced with increasing water content. Overall, the lowest H_2 FEs of 16% were recorded with the combination of relatively high Nafion content of 0.25 wt% and high water content of 50–75 vol% (Figure 3a). Accordingly, the selectivity toward CO_2R was significantly enhanced in this catalyst ink composition range, with the FEs of C_2H_4 increasing to ≈58% (Figure 3b). Similarly, the production of ethanol, another major C_2 product, was also promoted in the region of both high Nafion (0.25-0.5 wt%) and water content (25-75 vol%), with FEs reaching above 20% (Figure 3c). The FEs for other C_{2+} products, such as acetate and n-propanol (denoted as PrOH), were below 5% on all electrodes and represented a minor contribution to the total CO_2R product distribution (Figure S8f,h, Supporting Information). Thus, the production of C_{2+} products was maximized with a FE of ≈84% and a partial current density of approximately -10 mA cm^{-2} on electrodes prepared with inks containing 0.25 wt% Nafion and >25 vol% water (Figure 3d,e).

In contrast to the case of C_{2+} products, the selectivities of single carbon (C_1) products such as CO and CH_4 were very low on all electrodes, with FEs of <1.8% for CO and <3.7% for CH_4 (Figure S8b,c, Supporting Information). Formate was the only comparatively major C_1 product and its FE exhibited a strong dependence on Nafion content. Specifically, increasing Nafion content resulted in decreasing formate production regardless of water content, and the corresponding FE was reduced from a peak value of 7.6% at 0.005 wt% Nafion to 1% at 0.5 wt% Nafion (Figure S8d, Supporting Information). Considering the minimal FEs of both CO and CH_4, the overall production of C_1 products was therefore predominantly influenced by Nafion content (Figure S9b, Supporting Information). Consequently, as shown in Figure S9d (Supporting Information), the ratio of C_{2+} FE to C_1 FE (C_{2+}/C_1) also displayed a strong dependence on Nafion content.

As discussed above, increased Nafion content leads to thicker Nafion coatings, suggesting that the competition between C_{2+} and C_1 reaction pathways can be modulated by tuning the thickness of Nafion coatings. Indeed, it has been shown that thick Nafion films can raise local pH values by trapping hydroxide ions (OH^-) generated during CO_2 electrolysis and preventing buffering bicarbonate species from entering the local microenvironment, thereby enhancing C_{2+} selectivity.[13] However, thicker

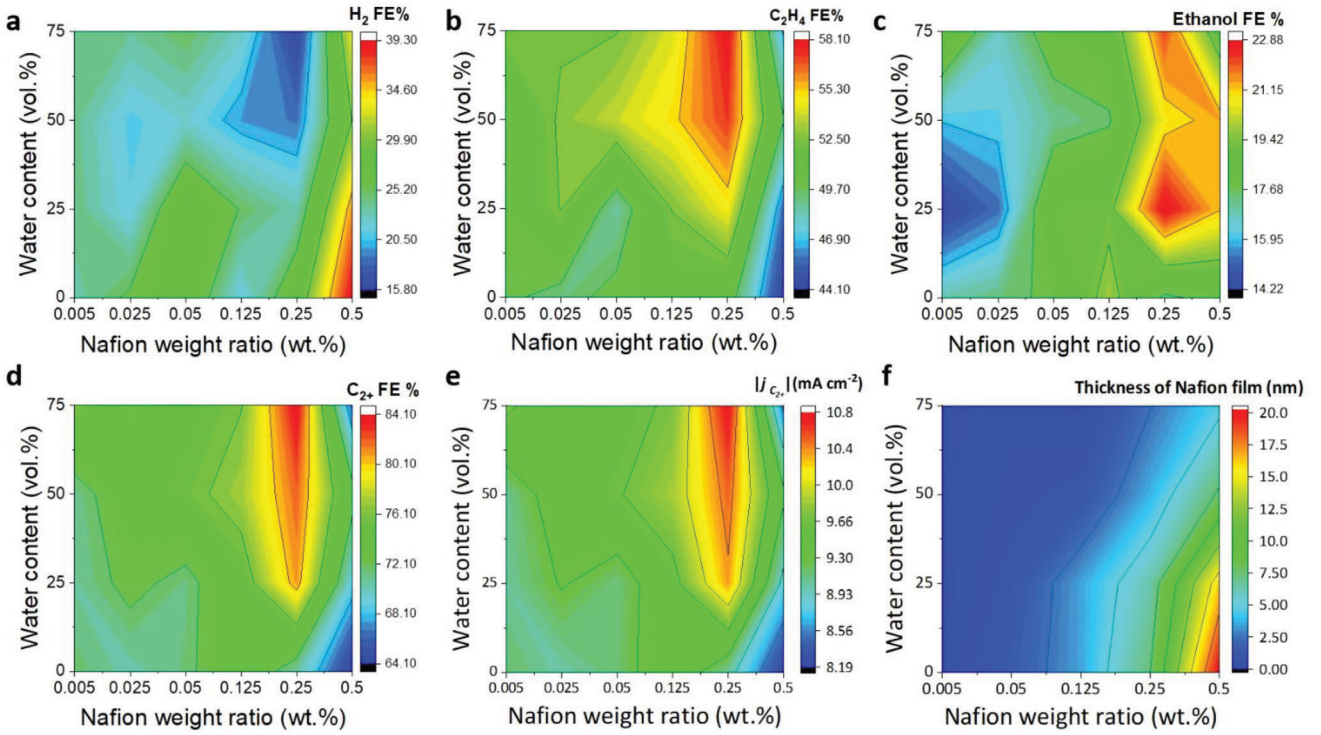

Figure 3. Analysis of the impact of catalyst ink composition on selectivity, activity, and thickness of Nafion coatings. Heatmaps of Faradaic efficiency for H_2 a), C_2H_4 b), ethanol c), and C_{2+} products d), as well as partial current density for C_{2+} products e), during chronopotentiometric CO_2 electrolysis at -12.8 mA cm^{-2} on glassy carbon compared to the thickness of Nafion coatings f), prepared from dispersions with varied Nafion contents and solvent compositions.

ionomer coatings can also block active sites, as evidenced by electric double layer capacitance measurements (Figure S4, Supporting Information) and may also leads to inefficient mass transport at the catalyst/electrolyte interface. To better understand these competing effects on C_{2+} FE, Figure 3f shows a heatmap of Nafion thickness as a function of catalyst ink composition. As expected, the thickness increases with increasing Nafion and decreasing water content. Comparison of the thickness heatmap to the product distribution heatmaps reveals a clear trend of increasing H_2 and decreasing C_{2+} product generation with increasing Nafion thickness, indicating that thicknesses of >10 nm are detrimental. In contrast, while the yield of C_{2+} products is enhanced for catalyst inks containing both high water and Nafion contents, resulting in Nafion films of ≈2.5–7.0 nm (Table S1, Supporting Information), no clear trend between thickness and electrocatalytic properties is observed. However, as previously reported, the increasing solvent dielectric constant with increasing water content also leads to improved network connectivity and reduced water uptake within the Nafion films, which is consistent with atomic force microscopy (AFM) analysis (Figure S10, Supporting Information). Thus, the C_{2+} product partial current density peaks at -10.8 mA cm^{-2}, realized with an ink composition of 75 vol% H_2O-0.25 wt% Nafion (Figure 3e), which yields a favorable balance of thickness and internal Nafion structure.

Finally, we note that the heatmap profiles for both C_2H_4 and ethanol exhibit a striking similarity, which is reasonable considering that they share the same critical intermediate, *CO, in their respective reaction pathways. This aligns well with the observed trends seen in heatmaps for all C_{2+} products (Figure S9, Supporting Information), where the hot spots (with high FEs) for each C_{2+} product are consistently located in the regions with low CO FEs, suggesting efficient C-C coupling rather than release of CO. Overall, we find that the optimal catalyst ink compositions for not only selective CO_2R but also enhanced production of C_{2+} products involve a combination of high water content (>50 vol%) and relatively high Nafion content (i.e., 0.25 wt%).

2.3. Stabilized C_{2+} Selectivity During Long-Term CO_2 Electrolysis

Having obtained a maximum C_{2+} FE of 84% during 5 h of continuous CO_2 electrolysis using the working electrode prepared from a catalyst ink containing 75 vol% H_2O-0.25 wt% Nafion, we subsequently assessed its durability during 200 h of chronopotentiometric CO_2 electrolysis at -12.8 mA cm^{-2}. As described in the Experimental Section, this long-term stability test was performed in five sequential experiments of ≈40 h duration, immediately following one another, in order to allow the electrolyte to be periodically refreshed. For comparison, a second electrode was prepared from a catalyst ink containing 0 vol% H_2O-0.25 wt% Nafion and was tested under identical conditions. Immediately prior to the long-term electrolysis experiments, the potential-dependent performance characteristics of both electrodes were confirmed by performing 5 h chronoamperometric tests (**Figure** 4a–c). Compared to the 0 vol%-0.25 wt% electrode, the 75 vol%-0.25 wt% electrode delivered higher TCDs over the potential range from

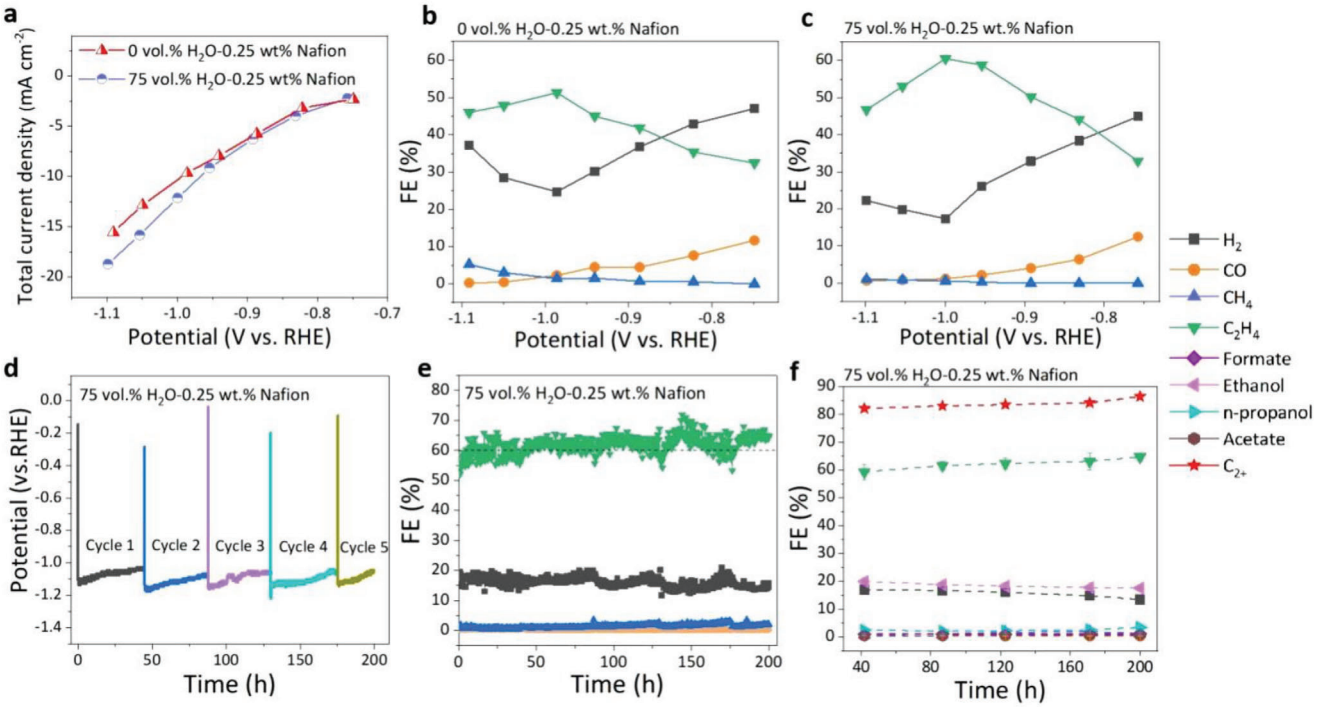

Figure 4. a–c) Potential-dependent performance of two electrodes prepared with 0.25 wt% Nafion and different water contents (0 and 75 vol%) in terms of total current densities (a) and Faradaic efficiencies (FEs) of gas products (b, c). d,e) Evaluation of durability in 200 h chronopotentiometric CO_2 electrolysis at -12.8 mA cm^{-2} on the electrode prepared from the ink containing 75 vol% H_2O and 0.25 wt% Nafion. The dynamic change of cathodic potential (d) and FEs of gas products measured every 20 min over 200 h (e). f) The average FEs of all products in each cycle of ≈40 h.

-0.9 to -1.1 V_{RHE}, as well as higher C_2H_4 FEs and much lower H_2 FEs across the complete range of investigated potentials. These findings are consistent with the conclusions discussed above that high water content catalyst inks contribute to suppressed HER and enhanced generation of C_{2+} products.

Throughout the entire course of the 200 h long-term durability test, the 75 vol% H_2O-0.25 wt% Nafion electrode exhibited high FEs for CO_2R (Figure 4e,f). The corresponding operating potential was also stable, near -1.10 V_{RHE}, decreasing slightly to approx. -1.05 V_{RHE} with time (Figure 4d). Surprisingly, the C_2H_4 FE increased from ≈55% at the beginning of the chronopotentiometric experiment to ≈60% after 40 h of operation, eventually reaching a peak average FE of 65% during the last 30 h of testing. This represents an overall relative increase of the C_2H_4 FE of ≈19% (≈10% absolute increase) during 200 h of sustained operation. The increased C_2H_4 FE was accompanied by progressively decreased FEs for the production of both H_2 and ethanol, with the averaged FEs of H_2 decreasing from 17% to 13% and of ethanol decreasing from 20% to 17%.

Previous mechanistic studies have revealed that the selective production of C_2H_4 and ethanol is determined by the C-C coupling process and the subsequent hydrodeoxygenation of C_2 intermediates, respectively.[27] The C_2H_4 selectivity can therefore be enhanced by engineering catalyst structures (facets, defects, nanostructures) to promote C-C coupling, as well as by modulating local reaction environments at the catalyst interface (pH, CO_2/H_2O availability, CO coverage, and electrolyte cation).[9,13,16,27–31] In contrast, achieving high ethanol selectivity is difficult on pure Cu catalysts and typically requires bimetallic synergy or surface modification strategies to enhance the C-O bond strength or the relative stability of intermediates on the ethanol-forming pathway.[27,32–35] Given the pure CuO-derived catalysts used here, as well as the comparatively minor decrease of ethanol FE with operational time, we infer that the constant rise of C_2H_4 selectivity during the 200 h chronopotentiometric test is primarily driven by enhanced C-C coupling rather than an increase of the hydrodeoxygenation efficiency. In addition, we note that the production of all other minor products, including CO, CH_4, formate, acetate, and n-propanol, was maintained at minimal levels, accounting for FEs in the range of just 0.5% to 3%. The FE of C_{2+} products hence exhibited a steady increase over the course of 200 h and reached a remarkable value of 86% by the conclusion of the experiment. As summarized in **Table 1**, this represents one of the highest C_{2+} FEs and longest stabilities for long-term liquid phase aqueous CO_2R reported to date. Importantly, the majority of studies report durability tests of Cu-assisted CO_2 electrolysis for operational periods of less than 10 h due to the inevitable degradation of catalytic activity. In contrast, we find no evidence for degradation during 200 h of testing and, on the contrary, observe an increase of selectivity and decrease of operating potential during extended testing.

To better understand the remarkable combination of selectivity and stability achieved by these Nafion-coated Cu nanoparticle catalyst layers, we compare the long-term performance characteristics of the optimal 75 vol%-0.25 wt% electrode with that of the 0 vol%-0.25 wt% electrode (Figure S11, Supporting Information). While the cathode formed from the 0 vol%-0.25 wt% ink composition also demonstrated reasonable stability, the FEs

Table 1. Comparison of optimized production of C_{2+} products on various Cu-based catalysts in neutral-pH aqueous electrolyte.

Catalyst	Nafion wt%/Water vol%	Electrolyte	Substrate	Cathode Potential [V_{RHE}]	FE % C_2H_4/C_{2+}	Current Density [mA cm^{-2}]	Durability [h]	Refs.
Cu foil	0/N/A	0.1 M $KHCO_3$	Cu foil	−0.98	30/42	−5	0.5	[5]
		0.1 M KCl		−1.03	47.8/73.3	−5	0.5	
Oxidized Cu foil	0/N/A	0.1 M $KHCO_3$	Cu foil	−1.0	9.9/18.5	−5	1.2	[36]
Plasma treated Cu foil	0/N/A	0.1 M $KHCO_3$	Cu foil	−0.92	57/N/A	−12	5	[37]
CuO NPs	0/N/A	0.5 M $KHCO_3$	glassy carbon	−0.95	20/57	−30	5	[38]
Branched CuO NPs	5/0	0.1 M $KHCO_3$	glassy carbon	−1.05	65/65.5	−20 to -30	12	[39]
Cu_2O-derived Cu NPs,	0/N/A	0.1 M $KHCO_3$	Cu disc	−1.03	43/N/A	−31.2	1.2	[40]
18 nm				−1.03	10/N/A	−31.2	1.2	
41nm								
Cu_2O NPs, 2–4 nm	0.15/0	0.1 M $KHCO_3$	glassy carbon	−1.10	57/74	−17	10	[41]
Cu NPs, 10–40 nm	0/0	0.1 M $CsHCO_3$	carbon paper	−0.75	30/50	−20	10	[42]
Plasma treated Cu nanocubes	0/N/A	0.1 M $KHCO_3$	Cu foil	−1.0	44/64	−34	1	[43]
Cu_mCeO_x	0.12/50	0.1 M $KHCO_3$	glassy carbon	−1.10	>40/N/A	−3.2	6	[44]
Boron-doped Cu	0.10/0	0.1 M $KHCO_3$, 0.1 M KCl	glassy carbon	−1.10	52/79	−60 to −100	40	[45]
Cu nanowires	0.05/0	0.1 M $KHCO_3$	glassy carbon	−1.01	61-72/N/A	−22.4	205	[46]
Defective Cu nanosheets	0.24/0	0.1 M K_2SO_4	glassy carbon	−1.18	80/N/A	−60	14	[47]
CuO NPs, 50 nm	0.25/75	0.1 M $KHCO_3$	glassy carbon	−1.05	60-65/86	−12.8	200	This work

of both C_2H_4 and ethanol were significantly lower than those measured on the 75 vol%-0.25 wt% cathode, exhibiting stabilized values over the 200 h test of ≈50% and 12%, respectively (Figure S11b,c, Supporting Information). Furthermore, this electrode was characterized by a nearly 2× larger H_2 FE, which gradually increased from 28% to 31% during the long-term stability test (Figure S11b, Supporting Information). The FE of C_{2+} products was ≈65%, which is more than 20% lower than that found for the 75 vol%-0.25 wt% electrode as described above (Figure 4f; Figure S11c, Supporting Information). Importantly, the sole difference between these two electrodes is the water content of the solvent used in the catalyst ink, which is known to have a profound impact on the internal structure and thickness of the resulting Nafion coating. In particular, electrodes prepared from high water content solvents possess thinner Nafion coatings with improved inner network connectivity, resulting in significantly enhanced CO_2/H_2O local concentration ratios and greater OH^- accumulation that favors CO_2R over HER and promotes C-C coupling, respectively. In contrast, those prepared without water in the solvent tend to be thicker and are characterized by greater water uptake, resulting in lower CO_2/H_2O concentration ratios and increased HER. While detection of Nafion by transmission electron microscopy (TEM) after stability testing was challenging (**Figure** 5a,b) due to the ultrathin and amorphous nature of the coatings, complementary detection of fluorine by energy dispersive X-ray (EDX) spectroscopy verifies that Nafion is retained on both electrodes following sustained CO_2 electrolysis for 200 h (Figure S12, Supporting Information).

Although the favorable reaction microenvironment accounts for higher C_{2+} selectivity on the electrode prepared with 75 vol% water compared to that prepared with 0 vol% water, the reason for the progressive enhancement of the FE of C_{2+} products, especially C_2H_4, during the course of 200 h chronopotentiometric testing is not obvious. Here, we note that most previous studies on the stability of Cu-based catalysts report increasing HER and decreasing CO_2RR selectivity during sustained operation, typically on the order of 10 h (Table 1). A notable exception to this can be found in the work of Jung et al., who reported the in situ electrochemical fragmentation of Cu_2O NPs, with decreased particle size leading to a doubling of the FE of C_2H_4, from 27% to 57%.[41] Importantly, TEM analysis of catalysts from the two different electrodes indicates the presence of small particles (< 20 nm) in both cases (Figure 5a,b), suggesting that electrochemical fragmentation may proceed to some extent on both electrodes. To determine whether such a mechanism could be responsible for the increase of C_{2+} FE with time for our Nafion-coated CuO nanoparticles, we collected SEM images of the 75 vol%-0.25 wt% and the 0 vol%-0.25 wt% electrodes before and after 200 h of operation (Figure 5c,d). In both cases, the starting CuO NPs are well dispersed and are characterized by an average diameter of ≈50 nm (Figure S13, Supporting Information). While SEM indicates that this morphology and average size is largely preserved for the case of the 0 vol%-0.25 wt% electrode (Figure 5c), which exhibited increasing HER activity during sustained operation, a notable decrease of the average particle diameter is observed for the 75 vol%-0.25 wt% cathode (Figure 5d), with a large fraction of particles possessing diameters below 20 nm. This finding suggests that a similar electrochemical fragmentation process may be responsible for the improved performance of the 75 vol%-0.25 wt% electrode during 200 h of electrolysis. Furthermore, the comparatively low degree of electrochemical fragmentation for the 0 vol%-0.25 wt% electrode is consistent with its more common behavior, with increasing H_2 FE over a similar operational time.

Here, it is important to note that electrochemical fragmentation comprises two distinct processes: the breaking of Cu NPs into smaller particles and the growth of small Cu NPs through the

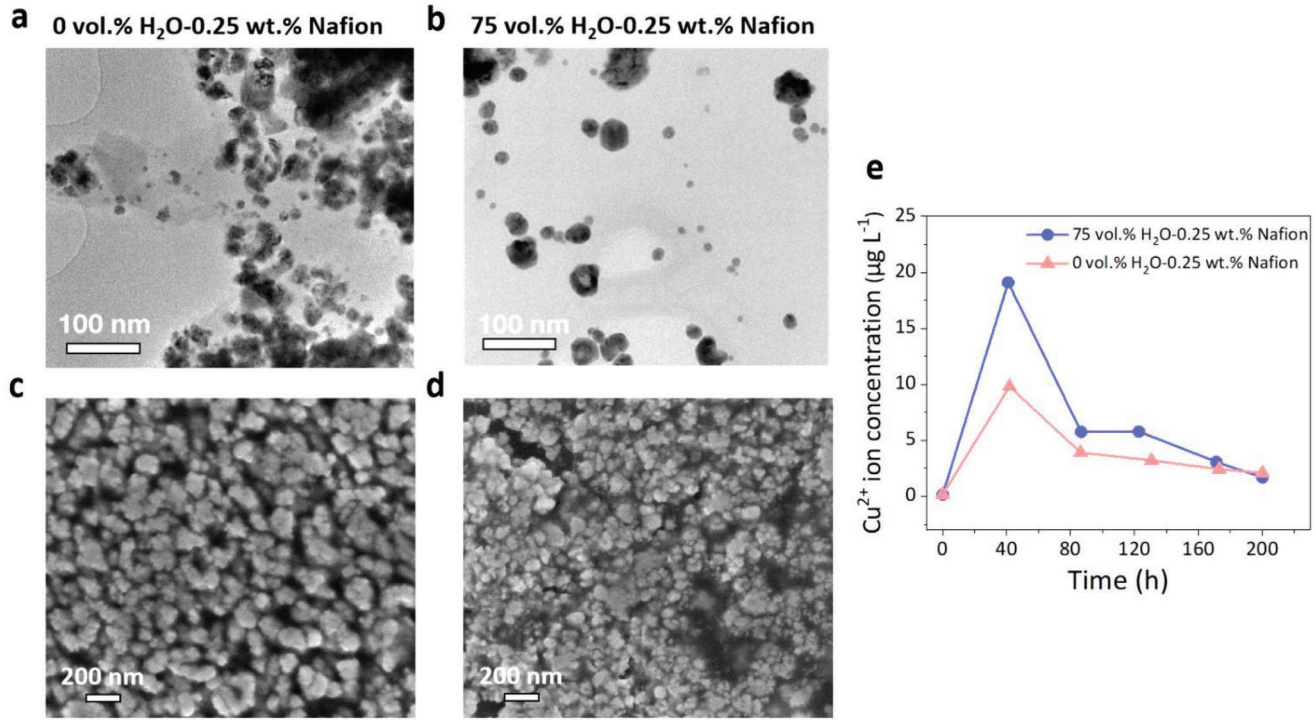

Figure 5. Characterization of catalyst layers and electrolytes after 200 h of CO_2 electrolysis. TEM a,b) and SEM c,d) images of catalyst layers prepared from inks with 0 vol% H_2O-0.25 wt% Nafion (a, c) and 75 vol% H_2O-0.25 wt% Nafion (b, d). e) Concentrations of dissolved Cu ions in electrolytes collected before electrolysis and after each cycle of CO_2 electrolysis measured by ICP-MS.

re-deposition of dissolved Cu species. These processes can collectively contribute to the overall fragmentation behavior. To better understand these phenomena, we analyzed the dissolved Cu^{2+} content in electrolytes as a function of electrolysis time using inductively coupled plasma mass spectrometry (ICP-MS). After the first cycle of ≈40 h, we detected a high Cu content for the best-performing electrode (75 vol%-0.25 wt%), with a Cu^{2+} concentration of 19.1 μg L^{-1} (Figure 5e). This concentration was nearly twice as large as the value of 9.8 μg L^{-1} obtained for the electrode prepared with the water-free formulation. Nevertheless, following continued operation, the dissolved Cu ion concentration dropped to lower levels of ≈5 μg L^{-1} Cu^{2+} for both electrodes, indicating redeposition on the cathode surfaces. These results indicate that catalyst particles with Nafion coatings fabricated from high water content ink formulations undergo a greater degree of dissolution and redeposition at the beginning of electrolysis, resulting in the generation of smaller nanoparticles. It has been demonstrated that such fragmentation or reconstruction of Cu catalysts can produce abundant undercoordinated sites near the surface, functioning as active sites to promote C-C coupling and, thus, enhancing the selectivity C_{2+} products, particularly C_2H_4.[6,7,28,41,46] In the present case, such a mechanism can also explain the observed increase of CO_2R performance during long-term operation for at least 200 h. It has been previously reported that such electrochemical fragmentation of Cu NPs typically occurs in the initial 5–6 h of operation and is closely related to three main factors, including the negative applied potential, the interaction between surface Cu atoms and intermediates in CO_2RR, and the local reaction environment (e.g., electrolyte).[41] Although the specific mechanism by which the catalyst ink composition and associated Nafion properties impact the electrochemical fragmentation process is not yet known, it is possible that the thicker Nafion films with poor inner network connectivity generated from water-free inks inhibit fragmentation by reducing the interaction between surface Cu atoms and CO_2R intermediates. While this hypothesis is consistent with the decreased electrochemically active surface area with reduced water content, additional in situ studies will be required to further clarify the complex interactions that govern fragmentation of hybrid Nafion/Cu catalyst layers.

2.4. Translation to Gas Diffusion Electrodes for Scalable CO_2 Electrolysis

Due to the low solubility of CO_2 in aqueous environments, CO_2 electrolysis is increasingly performed in flow cells or gas-fed MEAs incorporating GDEs, which enable significantly larger operational currents in scaled devices that are relevant for industrial applications. With this in mind, we next examined the general applicability of using optimized Nafion/solvent formulations to spray-coat Nafion/Cu nanoparticle catalyst layers onto GDEs and assessed their performance for CO_2 electrolysis in gas-fed MEAs. Based on the findings reported above, we chose to comparatively assess the performance characteristics of two such MEAs, derived from catalyst inks containing 75 vol% H_2O-0.25 wt% Nafion and containing 0 vol% H_2O-0.25 wt% Nafion. As shown in **Figure 6a**, the full cell voltages at the specified current

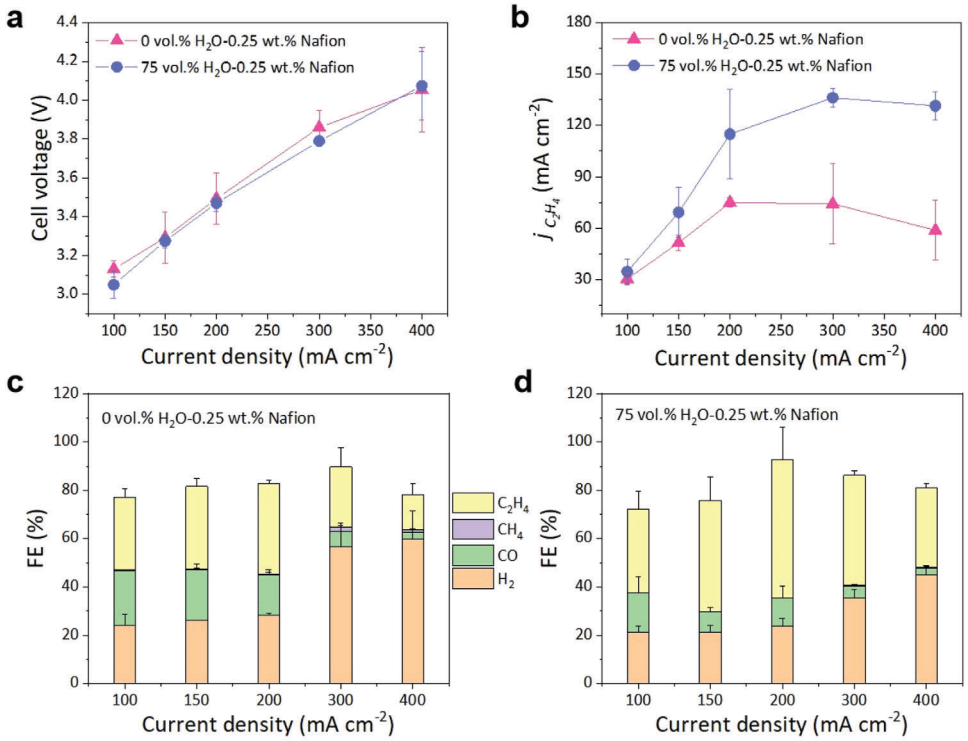

Figure 6. Current-dependent performance characteristics of gas-fed MEAs (active area 5 cm^2) using 0.1 M $KHCO_3$ aqueous solution as the anolyte. The cathodes were prepared with inks of 0.25 wt% Nafion and different water contents (0 and 75 vol%). The resulting cells were evaluated in terms of full cell voltages a), the partial current density of C_2H_4 b), and FEs of gas products c,d) examined in the galvanostatic mode at five different current densities, of 100, 150, 200, 300, and 400 mA cm^{-2}.

densities (100, 150, 200, 300, and 400 mA cm^{-2}) were similar in both cases, to within the experimental uncertainty. However, the high water content formulation yielded significantly higher partial current densities for C_2H_4 (Figure 6b), which were associated with dramatically suppressed FEs for H_2, CO, and CH_4 compared to the water-free ink formulation (Figure 6c,d). Quantitatively, the MEA produced with the optimal ink formulation reached a maximum C_2H_4 FE of 57.5% at a total current of 1 A (200 mA cm^{-2}), while the corresponding partial current density peaked at 136 mA cm^{-2}, measured at a total current of 1.5 A (300 mA cm^{-2}). This represents a 1.8-fold enhancement in the C_2H_4 yield rate compared to the maximum value (74 mA cm^{-2}) obtained on the electrode produced from the water-free solvent formulation (Figure 6b–d). Thus, we conclude that Nafion in high water content catalyst inks can positively influence C_{2+} selectivity, particularly C_2H_4, at industry-relevant current densities. As indicated by Table S2 (Supporting Information), the measured CO_2R to C_2H_4 performance characteristics reported here represent notable progress in scaling-up CO_2 electrolysis from proof-of-concept level (1 cm^{-2}) to larger area MEA CO_2 electrolyzers (5 cm^{-2}). While full optimization of such MEAs is outside the scope of the present work and is likely to also depend on a complex set of cell parameters within the complete cell, these results suggest that solvent-engineered Nafion/Cu nanoparticle catalyst layers can be applied to scalable CO_2 electrolysis systems operating at high current densities, including gas-fed MEAs.

3. Conclusion

In conclusion, we find that the exceptional CO_2R performance of Nafion-coated Cu-based catalysts arises from a complex interplay of several beneficial and synergistic factors that can be tuned via the catalyst ink composition. In particular, appropriately formed Nafion coatings can strike a careful balance between providing enhanced particle adhesion and reduced agglomeration to stabilize long-term performance, while also enabling in situ morphological reconstructions to achieve more active fragmented particle nanostructures. At the same time, the Nafion coatings provide favorable reaction microenvironments for suppressing HER and promoting C-C coupling. Here, the combination of high Nafion content and high water fraction in the solvent of the catalyst ink yields Nafion coatings possessing high inner network connectivity without significant blocking of surface sites, which is known to enable enhanced CO_2/H_2O concentration ratios and pH values in the local reaction microenvironment. Compared to our previously reported carbon paper supports, planar glassy carbon supports yield significantly higher FEs for C_{2+} products, which may be a consequence of the more homogeneous nanoscale structure. Overall, optimization of the Nafion content and the solvent composition of the catalyst ink yielded glassy carbon-supported CuO NP catalysts with Nafion coatings exhibiting remarkable FEs of 65% for C_2H_4 and 84% for C_{2+} products, along with excellent durability during 200 h of operation. Notably, the CO_2R performance, especially for the production of C_{2+} products, showed

continuous improvement over the 200 h testing period, reaching a total C_{2+} FE of 86% with no indications of performance degradation. This combination of high selectivity and durability is attributed to an increased loading of active sites for C-C coupling resulting from the electrochemical fragmentation of catalyst particles.

Despite the remarkable combination of selectivity and stability enabled by tailored Nafion coatings, we note that use of planar glassy carbon electrodes in an H-cell configuration introduces fundamental limitations to the maximum achievable current densities during CO_2 electrolysis. To overcome these restrictions, we extended this approach to MEA-based CO_2 electrolysis at industry-relevant current densities. In particular, we show that optimized catalyst ink formulations can be used to spray coat MEAs, resulting in scalable electrochemical CO_2 reduction systems featuring significantly enhanced C_2H_4 selectivity and activity. Thus, our findings present a straightforward and effective approach to engineer catalyst layers for highly selective and stable CO_2 electrolysis, including in gas diffusion electrode-based reactors.

4. Experimental Section

Preparation of Nafion Coatings and Working Electrodes: Catalyst inks were prepared using commercial Nafion ionomer dispersions (5 wt% in alcohol-water mixture containing 45% water + 55% propanol and methanol, Sigma-Aldrich), which were first diluted into 100% isopropanol or isopropanol-water solutions to achieve Nafion dispersions with different defined Nafion weight ratios. For example, 2 µL of the commercial Nafion dispersion was added to a solvent comprising 999 µL deionized water and 999 µL isopropanol, followed by 30 min of ultrasonic treatment, to make a specific Nafion dispersion with 50 vol% H_2O and 0.005 wt% Nafion. To complete the catalyst ink preparation, 10 mg of CuO powder (50 nm average diameter, Sigma-Aldrich) was added to each 2 mL Nafion dispersion.

To prepare cathodes, catalyst inks were deposited onto glassy carbon substrates (diameter of 5 mm, Gauss Union) with a working area of 0.196 cm^2. The mass loading of CuO catalyst was fixed at 0.255 mg cm^{-2}, which was obtained by drop-casting a total of 10 µL (2 µL, 5 times) of the catalyst ink onto the substrate. After drop casting, the electrodes were baked at 80 °C in air for 10 min on a hot plate. The Nafion weight ratios studied in this work were 0 wt%, 0.005 wt%, 0.025 wt%, 0.05 wt%, 0.125 wt%, 0.25 wt% and 0.5 wt%, and the investigated water contents in the solvent were 0 vol%, 25 vol%, 50 vol%, and 75 vol% (with the remaining fraction being isopropanol). Throughout this work, the prepared Nafion coatings and catalyst layers are denoted by their volumetric water content-Nafion weight ratio in the form of, for example, 75 vol%-0.25 wt%.

Physical and Chemical Characterization: Scanning electron microscopy (SEM, Zeiss NVision40 FIB-SEM) and transmission electron microscopy (TEM, FEI Titan ThemisG2 60–300, 300 kV) were used to analyze the morphologies of Nafion coatings and catalyst layers. For TEM analysis, the catalyst layers on the glassy carbon support were gently scratched away after 200 h of CO_2 electrolysis and transferred to a TEM grid (Cu grids from Plano, mesh 400 µm, 3 nm carbon film on lacey carbon). In a typical process, the catalyst coating was suspended in 10 µL ethanol, and 1 µL of the dispersed solution was dropped on the grid, followed by drying under an infrared lamp for ≈1 min. The collected grids were stored in a vacuum desiccator until TEM characterization. In addition, energy-dispersive X-ray (EDX) spectra were recorded using a four-quadrant Bruker SuperX chemiSTEM system to assess the presence of Nafion.

A Cu anode-equipped X-ray diffractometer (SmartLab, Rigaku) was utilized for crystallographic characterization in grazing incidence. The Cu content in electrolytes after long term CO_2 electrolysis was measured by inductively coupled plasma mass spectrometry (ICP-MS, Agilent 7900 ICP-MS) in the He-collision mode. The ICP-MS samples were prepared by diluting the electrolyte 5 times with a solution mixture of 2% HNO_3 and 0.5% HCl prepared from 70% HNO_3 and 35% HCl stock solutions (both CarlRoth, ROTIPURAN Supra, < 1ppb trace metals) and 18.2 MΩcm DI-water. The Cu calibration series was prepared from a certified multielement standard (TraceCERT, Transition Metal Mix 1) and the same mixture of 2% HNO_3 and 0.5% HCl.

Electrochemical Characterization: For CO_2 electrolysis in an H-type cell, an air-tight two-compartment H-type cell (C023-2, Gauss Union) with a Nafion 115 membrane separating the catholyte (45 mL) and anolyte (35 mL) was employed. All electrochemical measurements were performed using a potentiostat (Biologic VSP-300) connected in a three-electrode configuration, with a Ag/AgCl (filled with 3 M KCl) electrode (Gauss Union) and a Pt foil (99.99%, Gauss Union) electrode as the reference electrode and counter electrode, respectively. The working electrode and the reference electrode were placed at a defined constant distance from one another for all measurements.

The series resistance (R), measured by electrochemical impedance spectroscopy and the current interrupt method, was compensated by 85%. All potentials were converted to the RHE scale using the equation below, in which i was the current recorded during CO_2 electrolysis:

$$E_{RHE} = E_{Ag/AgCl} + 0.85\ \mathrm{R}\, i + 0.207\ \mathrm{V} + 0.059\ \mathrm{pH} \quad (1)$$

Prior to CO_2 electrolysis measurements, the 0.1 M $KHCO_3$ (99.95%, Sigma-Aldrich) aqueous electrolyte was continuously purged with CO_2 gas (99.999%, Linde) for 1 h, ensuring CO_2 saturation. Continuous CO_2 bubbling was maintained during all CO_2 electrolysis experiments at a constant flow rate of 40 sccm, controlled by a mass flow controller (MKS). The electrochemical activation of working electrodes was carried out by 20 cycles of cyclic voltammetry (CV) scans between -1.0 and -1.8 V versus the Ag/AgCl reference electrode. Chronopotentiometry tests were conducted for 5 h or 200 h, as indicated in the text, at a constant current density (-12.8 mA cm^{-2}) and chronoamperometry tests were conducted for 1 h at each of the fixed potentials. For long-term chronopotentiometric CO_2 electrolysis over a period of 200 h, the electrolytes in both the cathodic and anodic compartments were refreshed after each cycle of ≈40 hours. Notably, to minimize the influence of oxygen in air on the catalyst layers, the working electrode was quickly transferred into degassed electrolytes when refreshing electrolytes. Afterwards, both compartments were purged with CO_2 gas for 1 h before starting the next cycle of durability testing.

For GDE-based CO_2 electrolysis, the MEA reactor (Sci-Materials Hub) consists of a titanium anode plate and a cathode plate with flow fields, along with insulating gaskets, integrated into a compression cell. The geometric area of each flow field is 5 cm^2. An anion exchange membrane (PiperION, A40-HCO3, Versogen) was used to separate the anode and the cathode. The anode was made of iridium oxide coated on titanium mesh (IrO_x/Ti mesh, Suzhou Borui Anodes Industry Inc.). The cathode was prepared by spray-coating of CuO-based catalyst inks (prepared with two different formulations containing 5 mg mL^{-1} CuO powder: 0 vol% H_2O-0.25 wt% Nafion and 75 vol% H_2O-0.25 wt% Nafion) on gas diffusion layers (2.3 cm × 2.3 cm carbon paper with micro-structures, JNT20A6L, JNTG), followed by baking at 80 °C for 15 min to achieve a constant loading of ≈1 mg cm^{-2}. The 0.1 M $KHCO_3$ aqueous anolyte was circulated at a flow rate of 30 mL min^{-1} using a peristaltic pump. Humidified CO_2 gas, realized by flowing CO_2 gas through a homemade humidifier at room temperature, was fed into the cathode flow field at a rate of 40 mL min^{-1} using a mass flow controller (MC-Series, Alicat Scientific). A potentiostat (PTC-05100EW, 5 V-100 A, IPS China Ltd.) was used to apply constant currents to the MEA and record the cell voltages accordingly. No iR compensation was performed for the electrochemical measurements in of the MEAs. Gas products were analyzed by online gas chromatography (GC2060, Shenzhen Zhentai Tech Ltd.) during CO_2 electrolysis at each current setpoint (0.5, 0.75, 1, 1.5, 2 A) for 1 h. The gas flow rate at the outlet of the gas chromatographer was measured for calculation of Faradaic efficiencies of gas products.

CO_2 Reduction Product Analysis: Gaseous products (hydrogen, carbon monoxide, methane, ethylene, and ethane) were quantified using an online

gas chromatograph (GC, SRI 8610C) outfitted with both a thermal conductivity detector and a flame ionization detector. Ar (99.9999%, Linde) was used as the carrier gas. After CO_2 electrolysis, cathodic electrolytes were analyzed using ^{1}H nuclear magnetic resonance (NMR) spectroscopy (Bruker AV 500 HD) to identify the yield of liquid products, including methanol, formate, acetate, ethanol, and n-propanol. For this purpose, 400 µL of electrolyte and 100 µL of D_2O with 200 ppm dimethyl sulfoxide as the internal standard were mixed, after which the concentration of each liquid product was measured and quantified using predefined calibration curves. The corresponding Faradaic efficiency (FE) was determined according to:

$$FE = \frac{nFC}{Q} \quad (2)$$

where n is the number of electrons required to produce one molecule of the specified product, F is the Faraday constant of 96,485 C mol^{-1}, C is the measured quantity of product molecules in mols, and Q is the total number of electrons consumed by electrolysis.

Supporting Information

Supporting Information is available from the Wiley Online Library or from the author.

Acknowledgements

This project had received funding from the European Research Council (ERC) under the European Union's Horizon 2020 research and innovation programme (grant agreement No. 864234), the Deutsche Forschungsgemeinschaft (DFG, German Research Foundation) under Germany´s Excellence Strategy – EXC 2089/1 – 390776260, the Federal Ministry of Education and Research (BMBF, Germany) project number 033RC021B within the CO2-WIN initiative, and TUM. Solar in the context of the Bavarian Collaborative Research Project Solar Technologies Go Hybrid (SolTech). S.S. acknowledges support from the Alexander von Humboldt Foundation. R. Z. and K. M.-C. acknowledge funding from the Bavarian High-tech Agenda within the EQAP project.

Open access funding enabled and organized by Projekt DEAL.

Conflict of Interest

The authors declare no conflict of interest.

Data Availability Statement

The data that support the findings of this study are available from the corresponding author upon reasonable request.

Keywords

CO_2 electrolysis, copper nanoparticles, electrochemical stability, microenvironment engineering, morphological transformations, Nafion

Received: November 18, 2023
Revised: February 29, 2024
Published online: April 9, 2024

[1] O. S. Bushuyev, P. de Luna, C. T. Dinh, L. Tao, G. Saur, J. van de Lagemaat, S. O. Kelley, E. H. Sargent, *Joule* **2018**, *2*, 825.
[2] S. Nitopi, E. Bertheussen, S. B. Scott, X. Liu, A. K. Engstfeld, S. Horch, B. Seger, I. E. L. Stephens, K. Chan, C. Hahn, J. K. Nørskov, T. F. Jaramillo, I. Chorkendorff, *Chem. Rev.* **2019**, *119*, 7610.
[3] H. Shin, K. U. Hansen, F. Jiao, *Nat. Sustain.* **2021**, *4*, 911.
[4] M. Jouny, W. Luc, F. Jiao, *Ind. Eng. Chem. Res.* **2018**, *57*, 2165.
[5] A. Murata, Y. Hori, *Bull. Chem. Soc. Jpn.* **1991**, *64*, 123.
[6] J.-J. Velasco-Velez, R. v Mom, L.-E. Sandoval-Diaz, L. J. Falling, C.-H. Chuang, D. Gao, T. E. Jones, Q. Zhu, R. Arrigo, B. Roldan Cuenya, A. Knop-Gericke, T. Lunkenbein, R. Schlögl, *ACS Energy Lett.* **2020**, *5*, 2106.
[7] T. Möller, F. Scholten, T. N. Thanh, I. Sinev, J. Timoshenko, X. Wang, Z. Jovanov, M. Gliech, B. Roldan Cuenya, A. S. Varela, *Angew. Chem.* **2020**, *132*, 18130.
[8] A. Loiudice, P. Lobaccaro, E. A. Kamali, T. Thao, B. H. Huang, J. W. Ager, R. Buonsanti, *Angew. Chem., Int. Ed.* **2016**, *55*, 5789.
[9] S. Ringe, E. L. Clark, J. Resasco, A. Walton, B. Seger, A. T. Bell, K. Chan, *Energy Environ. Sci.* **2019**, *12*, 3001.
[10] T. H. M. Pham, J. Zhang, M. Li, T.-H. Shen, Y. Ko, V. Tileli, W. Luo, A. Züttel, *Adv. Energy Mater.* **2022**, *12*, 2103663.
[11] H.-Q. Liang, S. Zhao, X.-M. Hu, M. Ceccato, T. Skrydstrup, K. Daasbjerg, *ACS Catal.* **2021**, *11*, 958.
[12] L. Zhou, C. Li, J.-J. Lv, W. Wang, S. Zhu, J. Li, Y. Yuan, Z.-J. Wang, Q. Zhang, H. Jin, S. Wang, *Carbon Energy* **2023**, *5*, e328.
[13] C. Kim, J. C. Bui, X. Luo, J. K. Cooper, A. Kusoglu, A. Z. Weber, A. T. Bell, *Nat. Energy* **2021**, *6*, 1026.
[14] S. Popović, M. Smiljanić, P. Jovanovič, J. Vavra, R. Buonsanti, N. Hodnik, *Angew. Chem., Int. Ed.* **2020**, *59*, 14736.
[15] F. Li, A. Thevenon, A. Rosas-Hernández, Z. Wang, Y. Li, C. M. Gabardo, A. Ozden, C. T. Dinh, J. Li, Y. Wang, J. P. Edwards, Y. Xu, C. McCallum, L. Tao, Z.-Q. Liang, M. Luo, X. Wang, H. Li, C. P. O'Brien, C.-S. Tan, D.-H. Nam, R. Quintero-Bermudez, T.-T. Zhuang, Y. C. Li, Z. Han, R. D. Britt, D. Sinton, T. Agapie, J. C. Peters, E. H. Sargent, *Nature* **2020**, *577*, 509.
[16] X. Li, Q. Liu, J. Wang, D. Meng, Y. Shu, X. Lv, B. Zhao, H. Yang, T. Cheng, Q. Gao, L. Li, H. B Wu, *Chem* **2022**, *8*, 2148.
[17] J. C. Bui, C. Kim, A. J. King, O. Romiluyi, A. Kusoglu, A. Z. Weber, A. T. Bell, *Acc. Chem. Res.* **2022**, *55*, 484.
[18] T. Zhao, J. Li, J. Liu, F. Liu, K. Xu, M. Yu, W. Xu, F. Cheng, *ACS Catal.* **2023**, *13*, 4444.
[19] T. Zhao, X. Zong, J. Liu, J. Chen, K. Xu, X. Wang, X. Chen, W. Yang, F. Liu, M. Yu, Available at SSRN 4477080.
[20] F. P. García de Arquer, C.-T. Dinh, A. Ozden, J. Wicks, C. McCallum, A. R. Kirmani, D.-H. Nam, C. Gabardo, A. Seifitokaldani, X. Wang, Y. C. Li, F. Li, J. Edwards, L. J. Richter, S. J. Thorpe, D. Sinton, E. H. Sargent, *Science (1979)* **2020**, *367*, 661.
[21] S.-J. Shin, H. Choi, S. Ringe, D. H. Won, H.-S. Oh, D. H. Kim, T. Lee, D.-H. Nam, H. Kim, C. H. Choi, *Nat. Commun.* **2022**, *13*, 5482.
[22] Y. E. Kim, W. Lee, Y. N. Ko, J. E. Park, D. Tan, J. Hong, Y. E. Jeon, J. Oh, K. T. Park, *ACS Sustain Chem Eng* **2022**, *10*, 11710.
[23] L. de Sousa, C. Harmoko, N. Benes, G. Mul, *ACS ES&T Engineering* **2021**, *1*, 1649.
[24] P. Ding, H. An, P. Zellner, T. Guan, J. Gao, P. Müller-Buschbaum, B. M. Weckhuysen, W. van der Stam, I. D. Sharp, *ACS Catal.* **2023**, *13*, 5336.
[25] A. S. Varela, M. Kroschel, T. Reier, P. Strasser, *Catal. Today* **2016**, *260*, 8.
[26] X. Liu, P. Schlexer, J. Xiao, Y. Ji, L. Wang, R. B. Sandberg, M. Tang, K. S. Brown, H. Peng, S. Ringe, C. Hahn, T. F. Jaramillo, J. K. Nørskov, K. Chan, *Nat. Commun.* **2019**, *10*, 32.
[27] Z. Zhang, L. Bian, H. Tian, Y. Liu, Y. Bando, Y. Yamauchi, Z.-L. Wang, *Small* **2022**, *18*, 2107450.
[28] K. Yao, J. Li, H. Wang, R. Lu, X. Yang, M. Luo, N. Wang, Z. Wang, C. Liu, T. Jing, S. Chen, E. Cortés, S. A. Maier, S. Zhang, T. Li, Y. Yu, Y. Liu, X. Kang, H. Liang, *J. Am. Chem. Soc.* **2022**, *144*, 14005.

[29] R. Duan, L. Luo, W. Qin, X. Xiao, R. Zhou, Z. Zheng, *J. Phys. Chem. C* **2022**, *126*, 20878.
[30] X. K. Lu, B. Lu, H. Li, K. Lim, L. C. Seitz, *ACS Catal.* **2022**, *12*, 6663.
[31] W. Luo, X. Nie, M. J. Janik, A. Asthagiri, *ACS Catal.* **2016**, *6*, 219.
[32] H. Xu, D. Rebollar, H. He, L. Chong, Y. Liu, C. Liu, C.-J. Sun, T. Li, J. V Muntean, R. E. Winans, D.-J. Liu, T. Xu, *Nat. Energy* **2020**, *5*, 623.
[33] M. Luo, Z. Wang, Y. C. Li, J. Li, F. Li, Y. Lum, D.-H. Nam, B. Chen, J. Wicks, A. Xu, T. Zhuang, W. R. Leow, X. Wang, C.-T. Dinh, Y. Wang, Y. Wang, D. Sinton, E. H. Sargent, *Nat. Commun.* **2019**, *10*, 5814.
[34] H. Xu, D. Rebollar, H. He, L. Chong, Y. Liu, C. Liu, C.-J. Sun, T. Li, J. V Muntean, R. E. Winans, D.-J. Liu, T. Xu, *Nat. Energy* **2020**, *5*, 623.
[35] W. Ma, S. Xie, T. Liu, Q. Fan, J. Ye, F. Sun, Z. Jiang, Q. Zhang, J. Cheng, Y. Wang, *Nat. Catal.* **2020**, *3*, 478.
[36] Y. Lum, B. Yue, P. Lobaccaro, A. T. Bell, J. W. Ager, *J. Phys. Chem. C* **2017**, *121*, 14191.
[37] H. Mistry, A. S. Varela, C. S. Bonifacio, I. Zegkinoglou, I. Sinev, Y.-W. Choi, K. Kisslinger, E. A. Stach, J. C. Yang, P. Strasser, B. R. Cuenya, *Nat. Commun.* **2016**, *7*, 12123.
[38] A. Zahid, A. Shah, I. Shah, *Nanomaterials* **2022**, *12*, 1380.
[39] J. Kim, W. Choi, J. W. Park, C. Kim, M. Kim, H. Song, *J. Am. Chem. Soc.* **2019**, *141*, 6986.
[40] A. D. Handoko, C. W. Ong, Y. Huang, Z. G. Lee, L. Lin, G. B. Panetti, B. S. Yeo, *J. Phys. Chem. C* **2016**, *120*, 20058.
[41] H. Jung, S. Y. Lee, C. W. Lee, M. K. Cho, D. H. Won, C. Kim, H.-S. Oh, B. K. Min, Y. J. Hwang, *J. Am. Chem. Soc.* **2019**, *141*, 4624.
[42] D. Kim, C. S. Kley, Y. Li, P. Yang, *Proc. Natl. Acad. Sci. USA* **2017**, *114*, 10560.
[43] D. Gao, I. Zegkinoglou, N. J. Divins, F. Scholten, I. Sinev, P. Grosse, B. R Cuenya, *ACS Nano* **2017**, *11*, 4825.
[44] D. Wu, C. Dong, D. Wu, J. Fu, H. Liu, S. Hu, Z. Jiang, S. Z. Qiao, X.-W. Du, *J Mater Chem A Mater* **2018**, *6*, 9373.
[45] Y. Zhou, F. Che, M. Liu, C. Zou, Z. Liang, P. de Luna, H. Yuan, J. Li, Z. Wang, H. Xie, H. Li, P. Chen, E. Bladt, R. Quintero-Bermudez, T.-K. Sham, S. Bals, J. Hofkens, D. Sinton, G. Chen, E. H. Sargent, *Nat. Chem.* **2018**, *10*, 974.
[46] C. Choi, S. Kwon, T. Cheng, M. Xu, P. Tieu, C. Lee, J. Cai, H. M. Lee, X. Pan, X. Duan, W. A. Goddard, Y. Huang, *Nat. Catal.* **2020**, *3*, 804.
[47] B. Zhang, J. Zhang, M. Hua, Q. Wan, Z. Su, X. Tan, L. Liu, F. Zhang, G. Chen, D. Tan, X. Cheng, B. Han, L. Zheng, G. Mo, *J. Am. Chem. Soc.* **2020**, *142*, 13606.